Arsenic, manganese and aluminum contamination in groundwater resources of Western Amazonia (Peru)

Caroline M.C. de Meyer[1], Juan M. Rodríguez[2], Edward A. Carpio[2], Pilar A. García[2], Caroline Stengel[1], Michael Berg[1,*]

[1]Eawag, Swiss Federal Institute of Aquatic Science and Technology, 8600 Dübendorf, Switzerland; caroline.demeyer@eawag.ch; michael.berg@eawag.ch

[2]Facultad de Ciencias, Universidad Nacional de Ingeniería, Lima, Peru; jrodriguez@uni.edu.pe

* corresponding author, e-mail: michael.berg@eawag.ch

Abstract

This paper presents a first integrated survey on the occurrence and distribution of geogenic contaminants in groundwater resources of Western Amazonia in Peru. An increasing number of groundwater wells have been constructed for drinking water purposes in the last decades; however, the chemical quality of the groundwater resources in the Amazon region is poorly studied. We collected groundwater from the regions of Iquitos and Pucallpa to analyze the hydrochemical characteristics, including trace elements. The source aquifer of each well was determined by interpretation of the available geological information, which identified four different aquifer types with distinct hydrochemical properties. The majority of the wells in two of the aquifer types tap groundwater enriched in aluminum, arsenic, or manganese at levels harmful to human health. Holocene alluvial aquifers along the main Amazon tributaries with anoxic, near pH-neutral groundwater contained high concentrations of arsenic (up to 700 µg/L) and manganese (up to 4 mg/L). Around Iquitos, the acidic groundwater ($4.2 \leq pH \leq 5.5$) from unconfined aquifers composed of pure sand had dissolved aluminum concentrations of up to 3.3 mg/L. Groundwater from older or deeper aquifers generally was of good chemical quality. The high concentrations of toxic elements highlight the urgent need to assess the groundwater quality throughout Western Amazonia.

Keywords

geogenic contamination, drinking water, trace elements, Amazon River, Holocene, Iquitos

1. Introduction

The Amazon Basin is one of the largest, but also most poorly understood, hydrological regions on Earth. It covers about 40% of the South American continent and contains a human population of around 30 million. More than half of this population lives in urban centers and both people living in rural and urban areas partially rely on groundwater as a source of safe drinking water (UNEP, 2004). In the last decades, an increasing number of tube wells have been constructed for drinking water purposes in cities and in rural communities of Western Amazonia. Groundwater forms an essential alternative to surface water, which is subject to microbial and anthropogenic contamination as well as to seasonal fluctuations in availability and accessibility (UNEP, 2004). At present, the chemical quality of the groundwater resources in Western Amazonia are not well studied. This is of particular concern because of the indication that groundwater in this region might be naturally contaminated by arsenic under reducing aquifer conditions (Amini et al., 2008; Ravenscroft et al., 2009).

Arsenic is highly toxic, causing ailments ranging from skin lesions and cardiovascular disease to different types of cancer (Kapaj et al., 2006). Current global estimates indicate that some 150 million people consume groundwater containing arsenic concentrations above the WHO-limit of 10 µg/L (Ravenscroft et al., 2009), including in many places in South America (Bundschuh et al., 2012). One of the main processes identified for mobilization of arsenic in groundwater is reductive dissolution of Fe (hydr)oxides in reducing aquifer environments (McArthur et al, 2004; Smedley & Kinniburgh, 2002). Geogenic (natural) arsenic contamination of reducing aquifers has been recognized in many river basins and deltas around the world (Smedley & Kinniburgh, 2002; Ravenscroft et al., 2009). For example, the Bengal Basin and the Mekong and Red River deltas in South and Southeast Asia are some of the most widely known cases (Berg et al., 2001; Buschmann et al., 2008; Nickson et al., 1998; Smith et al., 2000; Stüben et al., 2003). The contaminated groundwater in these areas is mainly found in Holocene aquifers that are poorly drained and that contain reactive organic matter (Buschmann et al., 2007; McArthur et al., 2004; Meharg et al., 2006; Postma et al., 2012; Ravenscroft et al., 2001; Smedley & Kinniburgh, 2002; Winkel et al., 2008).

Western Amazonia shares some of the same features as these As-affected deltas and river basins. The main tributaries of the Amazon River originate in the relatively young, tectonically active Andean mountains and are known as whitewater or Andean rivers (Junk et al., 2011; Sioli, 1956). They carry substantial sediment loads (Kalliola et al., 1993; Mora et al., 2010; Syvitski et al., 2014) that are deposited in the sub-Andean basins of Western Amazonia (Räsänen et al., 1992; Roddaz et al., 2010) along with abundant natural organic matter (NOM). Recent neotectonic studies indicate that the Amazon region has been a dynamic depositional environment throughout the late Quaternary (Mora et al., 2010; Rossetti, 2014, and references therein). Large areas of Western Amazonia are therefore covered by Late-Pleistocene to Holocene deposits, mostly in fluvial terraces.

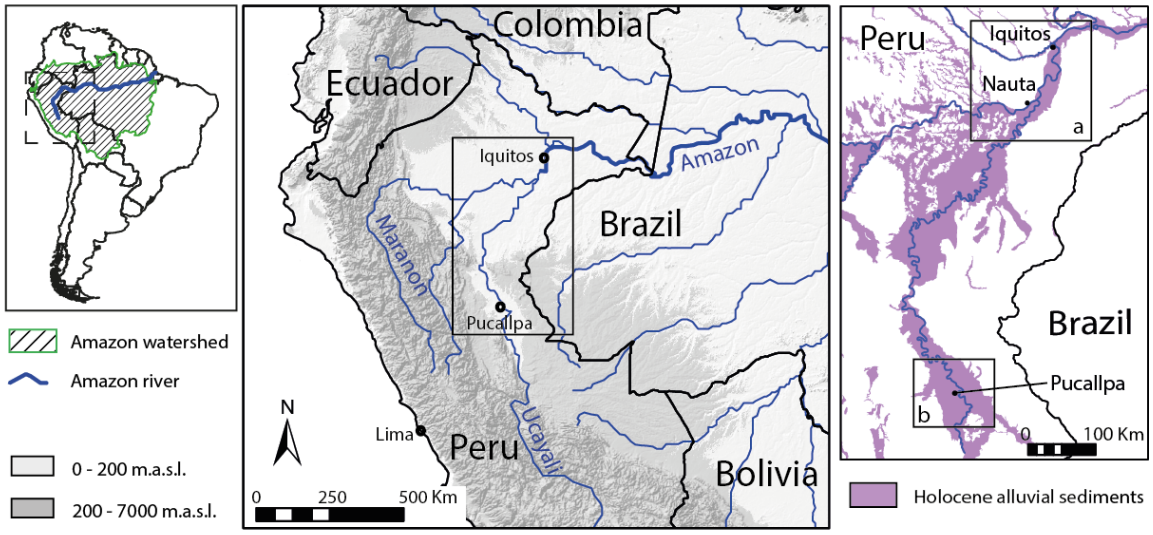

Fig. 1. Geographical locations of the study regions in the Peruvian part of the Amazon catchment. The squares in the right panel indicate (a) the region of Iquitos and (b) the region of Pucallpa. Amazonian tributaries originating in the Andes deposit large amounts of sediments in the floodplains of Western Amazonia. In the Holocene alluvial sediments, the probability for natural reducing aquifer conditions that can trigger mobilization of redox-sensitive trace elements such as arsenic and manganese, is high. Map sources: digital elevation model (DEM) from the Shuttle Radar Topographic Mission (SRTM) available from the U.S. Geological Survey; Mapa Geológico del Perú Escala 1:1 000 000 (INGEMMET, 1999).

The floodplains are seasonally inundated, resulting in the deposition of a fine silt-layer, and are poorly drained (Junk et al., 2011). Hence, in the floodplains of the main rivers (Figure 1) reducing

75 subsurface conditions that might trigger reductive dissolution of Fe(hydr)oxides in the aquifers are to
76 be expected. However, at the present time, little information is available regarding whether, where,
77 and to what extent this leads to the enrichment of arsenic and of other redox-sensitive elements
78 (e.g., manganese) in groundwater at concentrations harmful to human health. Groundwater
79 contaminants have been poorly investigated, with only a couple of studies reporting elevated
80 concentrations of As in water from tube wells in the Peruvian Amazon (e.g., Guzmán & Núñez,
81 1998a; Rebata-H et al., 2009).

82 Not all tributaries of the Amazon River originate in the Andes and carry high loads of sediments. In
83 Western Amazonia, the topographically elevated areas outside the floodplains of the whitewater
84 rivers are composed of older sediments of mainly Neogene age (Hoorn et al., 2010; Mora et al.,
85 2010). The blackwater rivers that originate in these areas (Kalliola et al., 1993; Klinge, 1967; Sioli,
86 1956) are characterized by low amounts of suspended material and low hardness, but high
87 concentrations of humic acids that give the acidic waters their typical dark brown color (Kalliola et
88 al., 1993; Junk et al., 2011; Sioli, 1956). The groundwater chemistry in areas drained by blackwater
89 rivers is expected to differ from that of whitewater basins.

90 In this study, we present a first comprehensive survey of groundwater quality in Western Amazonia
91 (Peru). We are aiming to verify the hypothesis that arsenic and other redox sensitive elements are
92 mobilized in reducing aquifers in recent sediments of the whitewater rivers. We also investigate the
93 presence of trace elements in aquifers in the vicinity of blackwater rivers. We further compare
94 groundwater in these young sediments with groundwater in older sediments. Finally, we discuss the
95 implications for the use of groundwater as a drinking water resource.

96 **2. Study regions and geology**

97 Figure 2 shows the two study regions we selected in the Amazon catchment of Peru, namely, the
98 areas of Iquitos and Pucallpa, the two largest cities in Western Amazonia. The geographical and
99 geological settings of both study regions are summarized below.

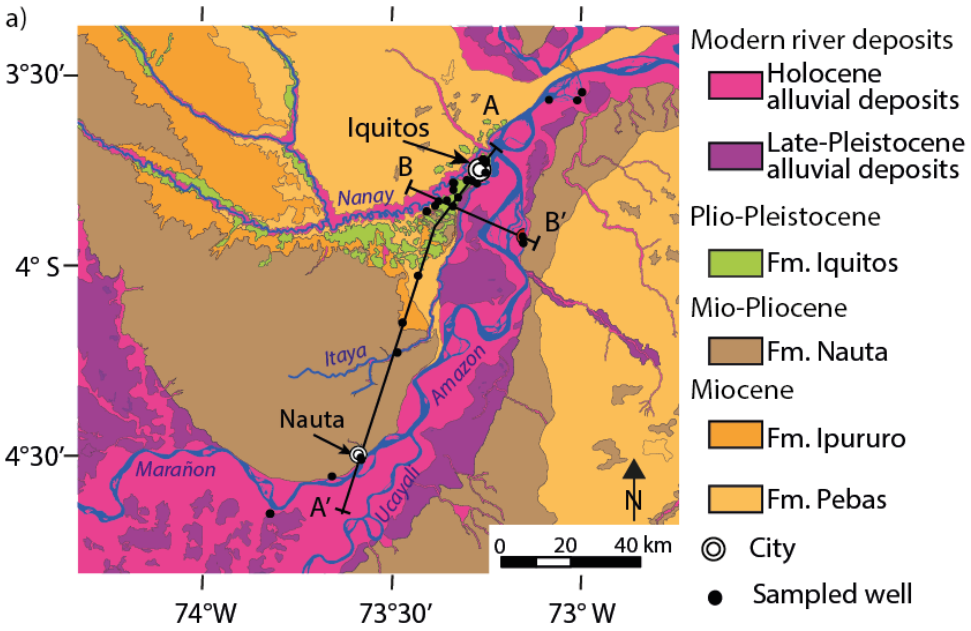

100

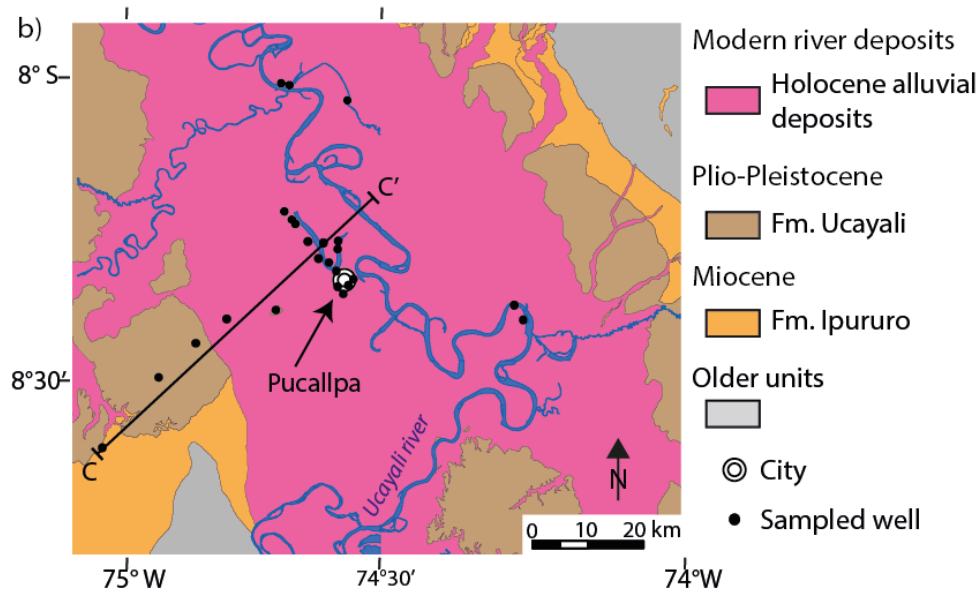

101

102 **Fig. 2.** Geological maps with indication of sampled wells of (a) study region Iquitos and (b) study
103 region Pucallpa. See Figure 1 for their locations. The indicated geological transects (A-A', B-B', and C-
104 C') are shown in Figure 3. Note that in panel (a) the division between Holocene (present floodplain)
105 and Late-Pleistocene alluvial deposits (terraces lying above the present-day flood level) is based on
106 geomorphology, with the latter age based on one determination by Dumont et al. (1988). Geological
107 maps adapted after De la Cruz (1997a,b), De La Cruz & Raymundo (1997), Guzmán & Núñez (1998b),
108 Martinez & Morales (1999 a,b), Monge & Valencia (1999 a,b,c,d), Romero & Raymundo (1999
109 a,b,c,d), and Sánchez et al. (1999 b,c).

110

2.1. Study region Iquitos

The study region of about 100 x 110 km^2 around the city of Iquitos (department of Loreto) was chosen because it covers various geological settings (Figure 2a). Iquitos is located on a Pleistocene terrace at the confluence of the main Amazon River and the Nanay River (Flores-P et al., 1998). The Nanay River is a small blackwater tributary that originates northwest of the study area, on Neogene sediments (Kalliola et al., 1993; Martínez et al., 1999; Puhakka et al., 1992). Hence, within a short distance, this area features both recent alluvial deposits from a whitewater river and a blackwater environment.

The population of Iquitos is about 440,000 (in 2015; INEI, 2012). Smaller settlements are scattered along the road connecting Iquitos and Nauta, a small town southwest of Iquitos (Figure 2a). Riverine communities are located both on the floodplains and on the higher lying areas. The climate is tropical, with an average yearly rainfall of ~2900 mm, and has no distinct dry season (Marengo, 1998). River levels rise and fall annually, thereby inundating parts of Iquitos and the riverine communities during the months of March–May (Sánchez et al., 1999a). The public water supply of the city of Iquitos draws water from the Nanay River for drinking water production (INRENA, 2006). However, many private and public institutions in Iquitos and in Nauta, as well as rural communities, use groundwater from shallow (5–45 m deep) tube wells as a drinking water resource.

The Iquitos study region covers four main geological formations (Figure 2a). The floodplains of the Marañon, Ucayali, and Amazon Rivers contain alluvial and fluvial sediments, with alternating clays, silts, and sandy silts deposited in a dynamic river system. We refer to these sediments as “modern river deposits.” The thickness of the deposits is variable and reaches several tens of meters. The age of the sediments spans from recent (Holocene) for the present floodplains to probably Late Pleistocene for deeper deposits and terraces above the yearly flooding level (Dumont et al., 1988; Sánchez et al., 1999a). The soils developed in exposed sediments of this formation are poorly drained, and are fertile due to the annual deposition of fresh silt (Paredes-G. A., 1998; Sánchez et al., 1999a).

137 The Iquitos Formation (Fm.), covering the terrace between the Nanay and the Itaya River (Figure 2a),
138 consists mainly of pure white quartz sands alternating with grey silty clays. The base can contain
139 conglomerates with silicified trunks and branches (Sánchez et al., 1999a). Some of the basal
140 conglomerates and sandy layers are reddish due to iron oxide cement. The thickness of the Iquitos
141 Fm. varies from about 10 to 50 m. These deposits, likely of Pleistocene age, form the elevated parts
142 of the region and fill up paleoreliefs in the underlying formations. These sediments were interpreted
143 as reworked highly weathered sands from Neogene sediments by the paleo-Nanay River (Räsänen et
144 al., 1998; Sánchez et al., 1999a). The soils developed in exposed sediments of this formation have
145 signs of strong tropical weathering, with podsolization to 10 m deep and the presence of alumina-
146 minerals such as gibbsite and kaolinite (Kauffman et al., 1998). In the floodplains of the Nanay River
147 and the Amazon River, the Iquitos Fm. is covered by recent alluvium. The sands and conglomerates
148 of the Iquitos Fm. form the main aquifer of the city of Iquitos (INRENA, 2006; Rüegg & Rosenzweig,
149 1949). The lower base of the aquifer corresponds to the contact of the Iquitos Fm. with the
150 impermeable clay layers of the underlying Pebas Fm.

151 The Nauta Fm. (Figure 2a) consists mainly of alternations of typically reddish or sometimes yellowish
152 coarse-grained sands and clays that fill up channels. The base of the sequences sometimes contain
153 gravel. The sediments are some 50 m thick and are generally highly weathered. Whether these
154 deposits are of Miocene age is subject to debate, as are its depositional environment and
155 geographical spread (Martínez et al., 1999; Rebata-H et al., 2006). Exposed sediments show strong
156 tropical weathering and kaolinite and Al-chloride are present (Martínez et al., 1999).

157 The Pebas Fm. (Figure 2a) is characterized by blue-grey to grey silty clays, alternating with some grey
158 and brown sandstones, carbonic layers, and shell layers. The most carbon-rich layers contain
159 botryoidal pyrite. At the top, red mudstones have been locally described (Sánchez et al., 1999a). The
160 sediments contain fossils that have been dated as Middle to Upper Miocene (Räsänen et al., 1998
161 and references therein). The geological map in Figure 2a distinguishes between the Ipururo Fm. and
162 the Pebas Fm. The Ipururo Fm. consists of 20–40 m thick, mainly grey, brown, and green sands, with

some silty and silty-clay layers and small calcareous concretions. The silts may be blackish due to organic carbon and may contain pyrites. The Ipururo Fm. mainly differs from the underlying Pebas Fm. by the absence of lignite layers and the presence of coarser grained material. The sediments of the Pebas and the Ipururo formations originated from the uplifting Andean mountain chain and were deposited in a fluvio-lacustrine environment with sporadic marine incursions from the north (Hoorn et al., 2010 and ref. therein; Rebata-H et al., 2006). Soils in these formations are mainly poorly developed (Kauffman et al., 1998; Sánchez et al., 1999a).

2.2. Study region Pucallpa

This study region of about 65 x 85 km^2 around the city of Pucallpa (department of Ucayali) is located on the large river plain formed by the Ucayali River, east of the Andes (see Figures 1 and 2b). Here, we verify the hypothesis of mobilization of arsenic in reducing aquifers in recent alluvial sediments deposited by a whitewater river. The population of Pucallpa is about 210,000 (in 2015; INEI, 2012). Rural communities and small towns are located along the rivers and lakes and along the main road connecting Pucallpa with Lima. The climate is tropical, with a yearly rainfall of ~1700 mm and a distinctly drier season from May to September (De La Cruz et al., 1997b). Part of the city and the riverine communities get annually flooded by the Ucayali River during February to April (De La Cruz et al., 1997b). In the city of Pucallpa, the public water supply distributes both surface water from the Ucayali River and groundwater from several deep wells (>100 m deep) (INRENA, 1998). Many other urban areas and rural communities use groundwater from their own mainly 60–100 m deep tube wells.

In this study region, three main geological formations are of interest to our study. More than half of the area is covered by recent alluvial and fluvial sediments deposited by the Ucayali River (see Figure 2b). The sediments consist of layers of dark silty sands and grey clays containing dispersed remains of trees and branches. The current alluvium is mainly composed of fine alternating layers of silts and clays. The sediments are Holocene in age and their thicknesses vary from several meters at the outskirts up to 50 meters in the actual floodplain (De La Cruz et al., 1997a,b).

These modern river deposits cover a thick clay formation, the so-called Ucayali Formation, which is composed of a sequence of mainly black, brown, and olive green clays with fossilized plant remnants and gastropods, alternating with some 4 to 5 m thick coarse sand layers with cross stratification (De La Cruz et al., 1997a,b). The base may show subhorizontal conglomeratic layers. The sand layers form the deeper productive aquifers in Pucallpa (INRENA, 1998). This formation is interpreted as Plio-Pleistocene in age and is about 50–100 m thick (De La Cruz et al., 1997a). In exposed sections, a thick soil layer has developed on top (De La Cruz et al., 1997a).

The Ipururo Formation (Figure2b) is characterized by fine grained grey or brown sandstones, with some hard iron sandstone concretions and dark shale layers. Layers of lignite, carbonized wood, and vertebrate fossils are present (De La Cruz et al., 1997a). The upper part is about 145 m thick and of Miocene to Pliocene age. Note that the Pebas and Ipururo Formations in the region of Iquitos correspond to the upper part of the Ipururo Fm. in the region of Pucallpa (De La Cruz et al., 1997b).

3. Materials and methods

3.1. Groundwater sampling

In both study regions, groundwater samples were collected from tube wells during a two-week sampling campaign in November 2016. Thirty-one samples were obtained from the Iquitos region and 26 samples from the Pucallpa region (see Fig. 2). Our aim was to obtain samples from throughout each field area, evenly distributed across each sedimentary unit. In practice, the sampling was strongly influenced by the availability and accessibility of the groundwater wells.

At each well, physico-chemical parameters (pH, T, O_2, EC, and Eh) were measured using a portable multi-analyzer (WTW Multi 340), with reported Eh values (mV) corrected against the standard hydrogen electrode. Water was pumped from tube wells with the available hand pump or electric pump. Using a hose, water was continuously pumped through a bucket in which the sensors were placed. The presence of any pronounced odors, such as hydrogen sulfide, were recorded. Where available, information on the depth of the well and the year of construction was provided by the well

owners. Fresh groundwater samples were taken from the outflow of the bucket after stabilization of EC and O_2, which required at least 10 minutes of pumping. Three aliquots per well were collected in PET flasks. One aliquot (30 mL) for analysis of major cations, trace elements, P and NH_4^+ was filtered on-site through disposable 0.45 µm nylon filters and acidified with supra pure 10 M HNO_3 to reach a pH of 1–2. A second aliquot (30 mL) was additionally passed through cartridges for arsenic speciation (Meng & Wang, 2008), between the filtration and acidification steps. The third aliquot (250 mL), for analysis of anions, alkalinity, total hardness, dissolved organic carbon (DOC), and total organic carbon (TOC), was collected unfiltered and non-acidified. The flasks were transported by airplane to our lab in Switzerland. Whenever possible, the samples were kept cooled and stored at 4°C in the dark prior to analysis.

3.2. Chemical analysis and quality assurance

The complete list of analyzed elements is available as Supplementary Information (Table SI1). The concentrations of major cations and trace elements were measured by inductively coupled plasma mass spectrometry (ICP-MS). Concentrations of NH_4^+, total P, and silicic acid were determined by photometry; Cl^-, SO_4^{2-}, and NO_3^- were measured with ion chromatography; total inorganic nitrogen was quantified with chemo luminescence; DOC and TOC were measured with a carbon-analyzer by catalytic combustion at 720 °C; and alkalinity and total hardness were determined by titration. Samples with measured total As concentrations greater than 1 µg/L were analyzed for As(III) concentrations by ICP-MS in the aliquot filtered for As speciation. The robustness of the ICP-MS element analysis was assured by intermittent measurement of groundwater reference samples from interlaboratory quality evaluations (i.e., ARS29 and 163F). These repetitive analyses agreed within ±5% of the known concentrations. In addition, cross-evaluation between ICP-MS and ion chromatography, carried out for the cations Na, K, Ca, and Mg, showed excellent agreement with coefficients of determination (r^2) ≥0.98. Calibration curves were r^2 >0.999. Standard deviations of triplicates were always <5%. The limits of quantification (LOQ, 10 x standard deviation of noise) are

239 listed in the Supplementary Table SI1 and were 0.5 µg/L for As and Mn, and 5 µg/L for Al. For more
240 details on quality assurance and data validation see Berg et al. (2008) and Winkel et al. (2011).

241 **3.3. Grouping of the aquifers based on interpretation of geology**

242 The sampled groundwater wells were grouped based on the geological formation that they tap.
243 Therefore, the source aquifer for each well was interpreted based on the depth of the well, its
244 location, and available geological information. The geological cross-sections (Figure 3) were
245 constructed using the following data — topography: digital elevation model (DEM) from the Shuttle
246 Radar Topographic Mission (SRTM) available from the U.S. Geological Survey; surface geology:
247 National geological maps of Peru at a scale 1:100.000 from INGEMMET (see references in Figure 2),
248 and for the geology at depth: the geological explicative notes of the geological maps (De la Cruz et
249 al., 1997a,b; Guzmán & Núñez, 1998a; Martínez et al., 1999; Sánchez et al., 1999a), and geological
250 sections in Räsänen et al. (1998), as well as field observations.

251 **4. Results**

252 **4.1. Aquifer types**

253 We were able to distinguish the following four aquifer types. Shallow tube wells (mainly <35 m deep)
254 located on the floodplains of the Amazon, Marañon and Ucayali Rivers in both study regions tap
255 groundwater from Aquifer Type 1, which corresponds to silty and sandy layers in the recent alluvial
256 sediments (Figure 3). The deeper tube wells (~60–100 m deep) in the study region of Pucallpa,
257 located in the floodplain and on the lowest terrace of the Ucayali River, tap groundwater from
258 Aquifer Type 2. Based on the well depth, the description of the aquifers in INRENA (1998), and the
259 geology (De La Cruz et al., 1997b), these wells pump groundwater from sandy layers of the
260 underlying Ucayali Fm. (Figure 3c). Aquifer Type 3 consists of the white sands of the Iquitos Fm. The
261 majority of the wells (5–28 m deep) located in the city of Iquitos and in the area between the Nanay
262 and the Itaya Rivers tap water from this unconfined aquifer (Figures 2a, 3a and 3b). Aquifer Type 4
263 groups the sandy and silty layers of the Neogene Nauta, Ipururo, and Pebas formations that are
264 tapped by tube wells in both study regions. Tube wells tapping groundwater from these aquifers

comprise both shallow and deeper wells on the terraces, as well as deeper wells on the floodplains of the main rivers (Figure 3).

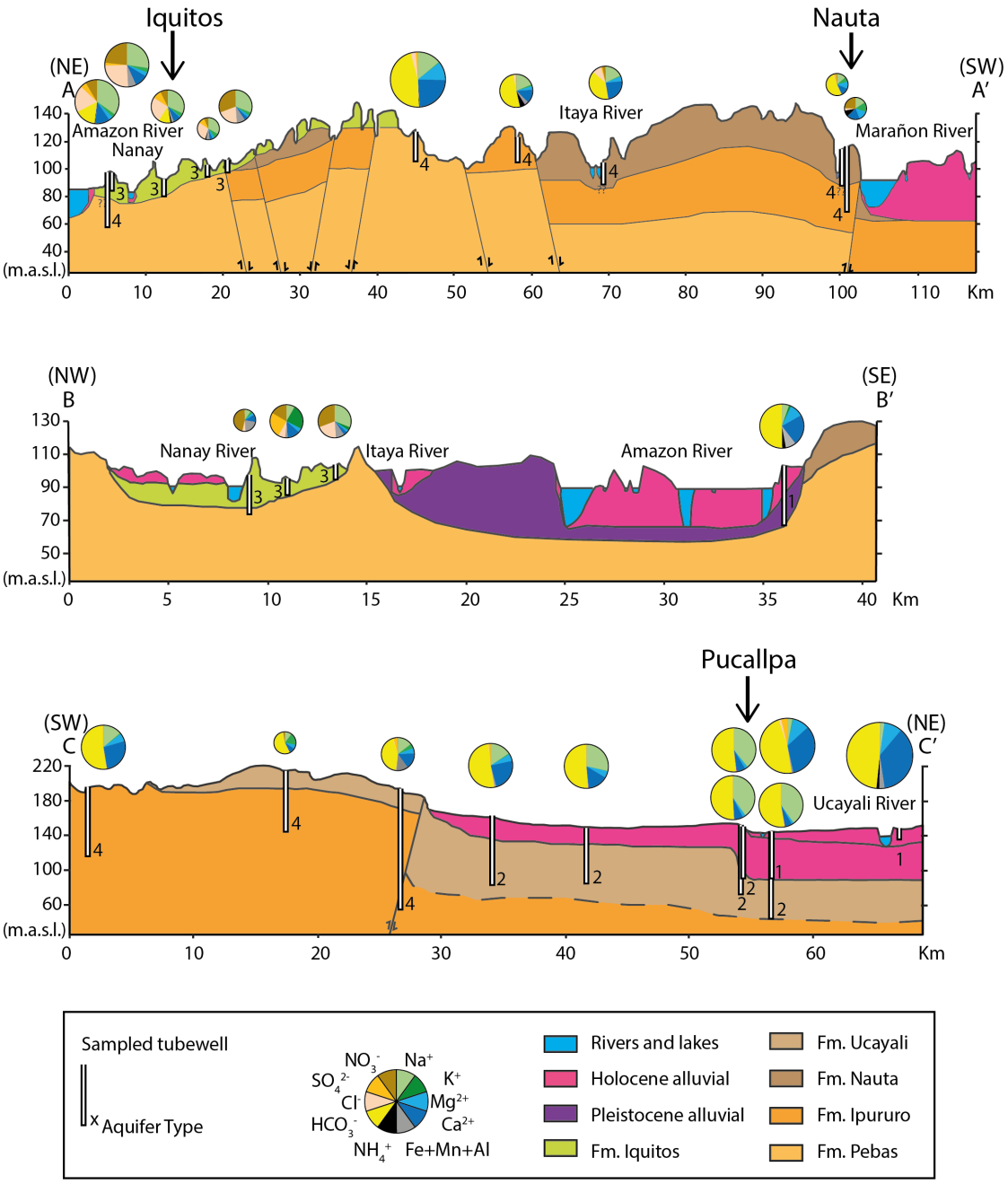

Fig. 3. Geological cross-sections with a selection of sampled groundwater wells along the transects in Figures 2a and 2b. The studied wells tap groundwater from four aquifer types. Aquifer Type 1 corresponds to the unconfined aquifers of the Modern river deposits in the floodplains of the Marañon, Ucayali and Amazon Rivers. Aquifer Type 2 includes sandy layers in the otherwise clayey Ucayali Formation. The white sands of the Iquitos Formation form Aquifer Type 3. In Aquifer Type 4 we grouped the sandy sediments of the Nauta, Ipururo and Pebas Formations. The pie-charts

illustrate the relative abundance (meq/L) of major anions and cations in the groundwater. The size of the pie-charts is tied to the electrical conductivity (range: <50; 50-150; 150-500; 500-1000; >1000 µS/cm).

4.2. Hydrochemistry

A summary of the chemical composition of groundwater from each aquifer type is given in Table 1. The complete data set of the 47 measured parameters is provided as supplementary information (Table SI1).

Table 1: Summary of the chemical composition of groundwater of each aquifer type.

	Aquifer Type 1			Aquifer Type 2			Aquifer Type 3			Aquifer Type 4		
Parameter	min.	max.	median	min.	max.	median	min.	max.	median	min.	max.	median
T (°C)	25.8	27.7	26.9	25.8	27.6	26.2	27.1	28.9	27.5	25.4	29.3	27.4
pH	6.4	7.1	6.8	6.4	8.1	7.8	4.2	5.5	4.6	4.8	7.6	6.1
Eh (mV)	64	196	109	46	295	109	146	598	555	119	626	409
Ec (µS/cm)	248	1226	494	219	1967	349	29	397	111	16	886	118
Al (µg/L)	< 5	< 5	< 5	< 5	16	< 5	17	3330	270	< 5	58	< 5
As (µg/L)	3	715	27	< 0.5	35	2	< 0.5	2	< 0.5	< 0.5	10	1
B (µg/L)	< 10	50	< 10	< 10	61	10	< 10	22	< 10	< 10	180	< 10
Ba (µg/L)	144	454	251	72	462	168	8	114	27	15	842	117
Ca (mg/L)	16	201	43	7	38	17	0	22	3	0	91	7
Cd (µg/L)	< 0.05	< 0.05	< 0.05	< 0.05	< 0.05	< 0.05	< 0.05	0.2	0.1	< 0.05	0.2	0.1
Ce (µg/L)	< 0.5	< 0.5	< 0.5	< 0.5	< 0.5	< 0.5	< 0.5	49	2	< 0.5	5	< 0.5
Cl^- (mg/L)	0.5	5.6	2.2	0.3	506	0.4	0.4	53	16	0.1	62	0.4
Co (µg/L)	< 0.1	1.8	0.1	< 0.1	0.3	< 0.1	< 0.1	7.4	0.3	< 0.1	1.8	0.7
Cr (µg/L)	< 0.1	0.8	< 0.1	< 0.1	0.2	< 0.1	< 0.1	0.3	< 0.1	< 0.1	1.4	< 0.1
Cu (µg/L)	< 0.2	3.6	< 0.2	< 0.2	8.6	< 0.2	< 0.2	3.4	1.1	< 0.2	6.2	0.4
DOC (mg/L)	0.5	16.4	2.6	< 0.5	1.1	0.6	< 0.5	1.8	0.8	< 0.5	2.0	<0.5
Fe (mg/L)	2.2	18.3	8.5	0.0	1.1	0.0	0.0	5.2	0.1	0.0	6.8	0.0
HCO_3^- (mg/L)*	137	808	277	140	385	226	0	24	0	13	543	58
K (mg/L)	2.2	10.4	5.0	0.5	1.5	0.8	0.3	13.7	1.9	0.4	9.3	2.2
La (µg/L)	< 0.5	< 0.5	< 0.5	< 0.5	< 0.5	< 0.5	< 0.5	27.5	0.6	< 0.5	2.1	< 0.5
Li (µg/L)	2.3	10	6.8	1.9	16.1	3.8	< 0.5	1.6	0.6	1	26.3	6.1
Mg (mg/L)	8	29	14	1	6	3	0	2	1	0	25	1
Mn (µg/L)	348	3689	1499	6	501	78	3	271	27	8	450	41
Mo (µg/L)	0.3	8.8	1	0.3	16.4	4.1	< 0.1	< 0.1	< 0.1	< 0.1	0.7	0.1
Na (mg/L)	7	40	12	17	327	66	1	36	11	0	71	7
NH_4-N (mg/L)	< 0.1	6.1	1.8	< 0.1	0.9	0.2	< 0.1	1	< 0.1	< 0.1	1.2	< 0.1
Ni (µg/L)	< 0.1	2.3	0.1	< 0.1	0.6	< 0.1	< 0.1	1.2	0.4	0.1	1.4	0.9
NO_3-N (mg/L)	< 0.05	< 0.05	< 0.05	< 0.05	0.2	< 0.05	< 0.05	16.6	2.1	< 0.05	10.6	0.1
N-tot (mg/L)	< 0.5	5.9	1.8	< 0.5	1.1	< 0.5	< 0.5	17.6	2.5	< 0.5	10.8	< 0.5
P (tot) (µg/L)	151	4003	931	< 25	447	156	< 25	< 25	< 25	< 25	200	< 25
Pb (µg/L)	< 0.2	< 0.2	< 0.2	< 0.2	0.7	< 0.2	< 0.2	5.0	0.5	< 0.2	0.7	< 0.2
Sb (µg/L)	0.1	1.0	0.1	0.1	0.2	0.1	0.1	0.2	0.1	0.1	1.2	0.1
Se (µg/L)	< 0.1	0.1	< 0.1	< 0.1	< 0.1	< 0.1	< 0.1	1.4	< 0.1	< 0.1	0.4	< 0.1
Si (mg/L)	17	49	43	7	27	9	2	5	3	4	29	13
SO_4^{2-} (mg/L)	< 0.5	22.1	< 0.5	< 0.5	3.4	< 0.5	< 0.5	28.8	1.9	< 0.5	19.1	0.8
Sr (µg/L)	120	1369	296	55	305	85	2	72	11	2	951	40
Tl (µg/L)	< 0.2	< 0.2	< 0.2	< 0.2	< 0.2	< 0.2	< 0.2	0.3	< 0.2	< 0.2	< 0.2	< 0.2
TOC (mg/L)	0.8	17.3	3.1	0.0	2.1	0.7	0.0	1.9	1.0	0.0	3.7	0.0
V (µg/L)	0.3	2.8	0.4	0.2	2.5	0.2	0.2	1.1	0.4	0.2	1.3	0.4
W (µg/L)	< 0.2	1.4	0.4	< 0.2	4.2	0.5	< 0.2	< 0.2	< 0.2	< 0.2	< 0.2	< 0.2
Zn (µg/L)	4	174	8	1	252	3	7	182	14	3	172	23

The concentrations of Sn (< 0.5 µg/L), Th (< 0.05 µg/L), U (< 0.05µg/L) were below detection limit for all samples.

*HCO_3^- concentrations were calculated based on alkalinity measured in non-acidified and non-filtered samples.

Note that the Eh values are corrected against the standard hydrogen electrode.

284 **4.2.1. Major elements**

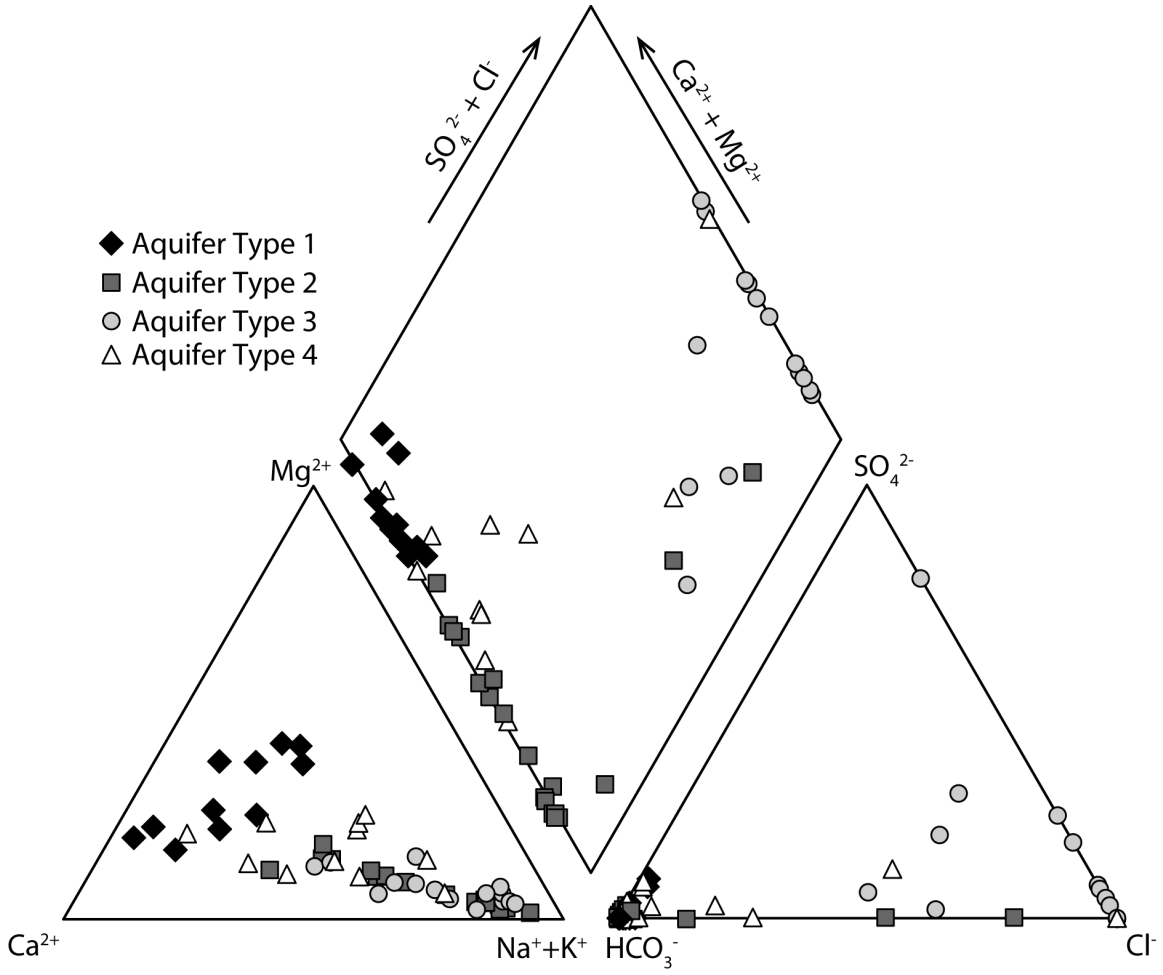

285

286 **Fig. 4.** Main groundwater chemistry presented in a Piper diagram. Groundwater of Aquifer Type 1 is
287 mainly of Ca-Mg-HCO_3^- type. Groundwater of Aquifer Type 2 is mainly of Na-Ca-HCO_3^- type, showing
288 a linear trend towards the Na-K pole. Some samples of Aquifer Type 2 are of Na-Cl type. Aquifer Type
289 3 shows the same trend as groundwater from Aquifer Type 2, but with Cl^- and SO_4^{2-} as main anions
290 instead of HCO_3^-. The samples from Aquifer Type 4 are mainly Na/Ca-HCO_3^- waters.

291 There was a large range of values of the hydrochemical parameters of the studied groundwater, but
292 distinct groups can be identified when considering the aquifer types separately. The different aquifer
293 types can be distinguished by the main cation and anion ternary plots in Figure 4, and by the Eh-pH
294 diagram in Figure 5. Groundwater of Aquifer Type 1 had mainly reducing, slightly acidic, Ca-Mg-HCO_3
295 properties within a pH range of 6.4 to 7.1. Aside from significant variability in Ca/Mg ratios (see
296 Figure 4), groundwater of Aquifer Type 1 was quite homogeneous in its main chemical

297 characteristics. Samples from both Aquifer Types 2 and 3 showed a trend in the main cation
298 distribution from Ca towards Na+K waters (Figure 4a). Samples from Aquifer Type 2 were mainly ion-
299 rich waters (with EC between 200 and 2000 µS/cm; see Table 1), plotting on the HCO_3^- - Cl^- tie-line,
300 whereas samples from Aquifer Type 3 are mainly ion-poor waters (with EC between 20 and 400
301 µS/cm; see Table 1), plotting towards the SO_4^{2-}-Cl^- tie-line (Figures 3 and 4). Both aquifer types were
302 also clearly distinguished in the Eh-pH plot in Figure 5. Aquifer Type 2 was mostly reducing, with a pH
303 ranging from 6.5 to 8.1., whereas groundwater from Aquifer Type 3 had a redox potential > 200mV
304 and a pH ranging from 4.2 to 5.5. The largest range of values was observed for the samples of Aquifer
305 Type 4, which is a heterogeneous group, ranging from acidic, oxidizing to slightly alkaline, reducing
306 waters (Figure 5). This water type varies from Ca-Mg-HCO_3^- to Na-Cl^-.

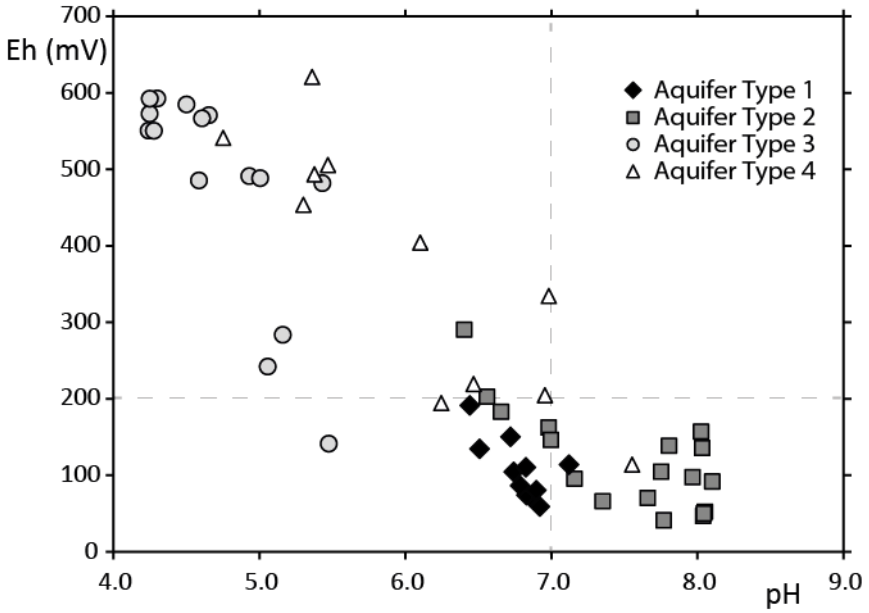

307

308 **Fig. 5.** Eh-pH diagram with sampled wells according to the aquifer type.

309 **4.2.2. Trace elements**

310 An overview of the trace element concentrations for each aquifer type is given in Table 1. Of all the
311 elements analyzed, arsenic, manganese, and aluminum were detected in concentrations of concern
312 to human health [i.e., exceeding the WHO-guideline or health based values of 10 µg/L (As), 400 µg/L
313 (Mn) and 900 µg/L (Al)] (WHO, 2011). Arsenic concentrations varied significantly, from less than 0.5

µg/L to a maximum of 715 µg/L; Mn-concentrations ranged from 3 µg/L to a max. of 4 mg/L and Al from less than 5 µg/L to a max. of 3.3 mg/L (see Table 1).

In general, distinct differences were seen between the aquifer types (Figure 6). The majority of the groundwater samples from Aquifer Type 1 had As concentrations above 10 µg/L, with one third exceeding 50 µg/L. At least 86% of the As was present as As(III) (see Table SI1). The Mn-concentrations exceeded 300 µg/L, with two thirds of the groundwater samples exceeding 1 mg/L. Groundwater of Aquifer Type 1 was further characterized by elevated concentrations of Fe, DOC, P, NH_4^+, and Si, when compared to the other waters in our dataset (see Figures 6 and 7). Ammonium showed a positive relation with As-concentrations >10 µg/L (Figure 7c). No such relation was observed for As with Fe or Mn (see Figures 7a and b), while sulfate and As associated negatively (see Fig. 7d). The Sr and Ba concentrations were generally higher in groundwater samples from Aquifer Type 1 than in the other aquifer types (see Table 1).

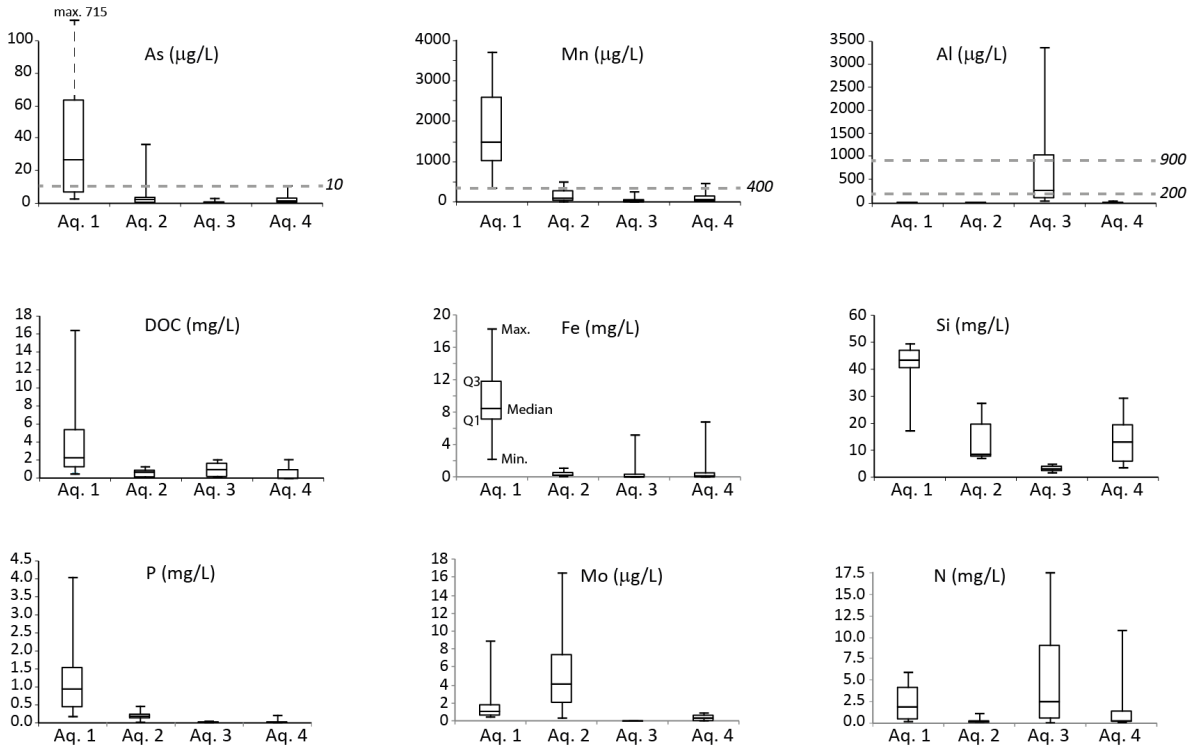

Fig. 6. Boxplot diagrams (Min.-Q1-Median-Q3-Max.) of selected elements. The samples are grouped per Aquifer Type. Number of samples: Aquifer Type 1 (11); Aquifer Type 2 (19); Aquifer Type 3 (15); Aquifer Type 4 (11).

With one exception, the groundwater of Aquifer Type 2 had As-concentrations below 6 µg/L. One third of the groundwater had Mn-concentrations above 200 µg/L, with a maximum concentration of 500 µg/L. The concentrations of P, DOC, and especially of Fe and NH_4^+ were also significantly lower than in Aquifer Type 1 (see Figures 6 and 7). The Mo-concentrations, with measured values up to 16 µg/L, were clearly higher than in the samples from the other aquifer types (see Figure 6).

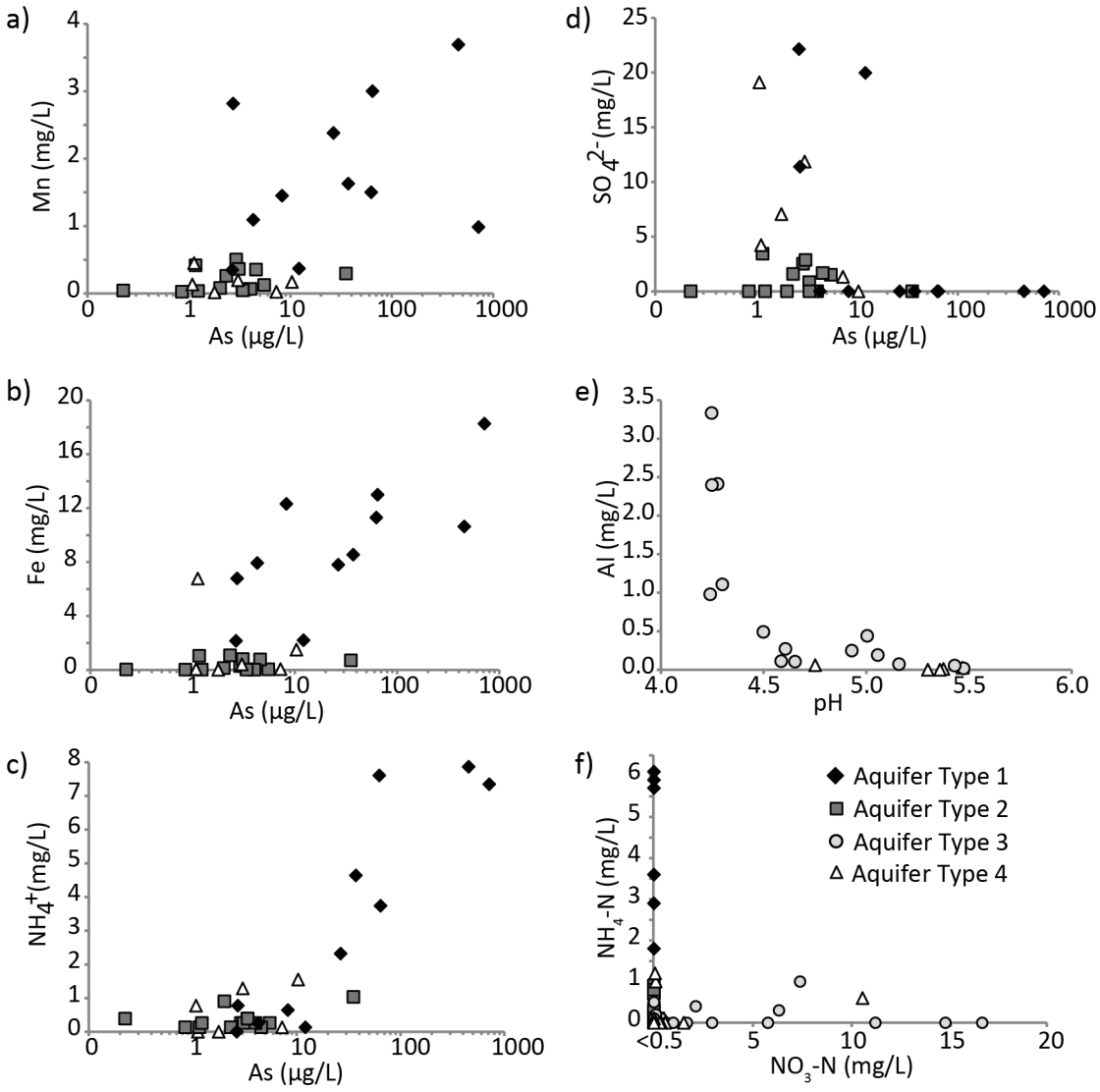

Fig. 7. Relationships between selected elements. (a, b) Mn, resp. Fe versus As in groundwater from Aquifers Types 1,2 and 4. Note that high As concentrations were accompanied by both high Fe and

high Mn concentrations. (c) NH_4^+ versus As in groundwater from Aquifer Types 1, 2 and 4. Note the positive relation between NH_4^+ and As for samples from Aquifer Type 1. (d) SO_4^{2-} versus As in groundwater from Aquifer Types 1, 2 and 4. No sulfate was detected for As concentrations >12 µg/L. (e) Al versus pH in groundwater from Aquifer Type 3. Note the negative relation between Al and pH, with a buffering of the pH at 4.2. (f) Ammonium versus nitrate. In Aquifer Types 1 and 2, all dissolved nitrogen was present as ammonium, whereas in Aquifer Type 3 nitrogen was mainly present as nitrate, except for the groundwater from wells in the area affected by flooding of the Amazon River.

The concentration of aluminum in groundwater from Aquifer Type 3 varied between <0.05 and 3.3 mg/L. In more than half of the groundwater samples, Al-concentrations exceeded 200 µg/L, and one third exceeded 900 µg/L (i.e., the WHO-health based value for drinking water) (WHO, 2011). A negative exponential correlation was noted with pH, with a maximum pH of 4.2 (Figure 7e). The samples were further characterized by low As, Mn, Fe, P, DOC, and Si concentrations. Nitrate concentrations ranged from below the detection limit to 17 mg NO_3-N/L (Figures 6 and 7), that is exceeding the WHO-guideline value of 11 mg NO_3-N/L (WHO, 2011). Groundwater of Aquifer Type 3 is slightly enriched in the elements La and Ce, and in the metals Pb and Cu, when compared with the other aquifer types (see Table 1). Three samples from wells in an area affected by flooding of the Amazon River differed by their lower redox potential (0 to 300 mV). They also displayed higher Fe (1.0–5.2 mg/L) and Mn (20–270 µg/L) and lower N (≤0.5 mg/L) concentrations when compared to the other samples from Aquifer Type 3.

Heterogeneity of the main hydrogeochemical characteristics was also observed for the trace element concentrations of Aquifer Type 4. Two wells tapping Aquifer Type 4 showed concentrations of Mn or As that slightly exceeded the WHO-guideline values. Groundwater containing ammonium generally had higher As, Fe, or Mn concentrations, and lower Eh-values. Nitrate was only present in groundwater with Eh-values >200 mV. We note that one sample had a concentration of Ba slightly exceeding the WHO-guideline value of 700 µg/L (WHO, 2011) (Table SI1).

5. Discussion

365 Table 2 presents an overview of the main characteristics of the four aquifer types and associated
366 geogenic contaminants. Elevated concentrations of arsenic and manganese were detected in
367 reducing, near-neutral pH groundwater mainly from Aquifer Type 1 (Figure 8a and 8b) [i.e., in the
368 recent sediments from whitewater rivers]. Elevated Al concentrations were only found in the oxic,
369 acidic groundwater from Aquifer Type 3 (Figure 8c) [i.e., in the sandy deposits of the Iquitos Fm.].

Table 2. Summary table with the main characteristics of the four aquifer types and associated geogenic contaminants

Aquifer Type	Geological Formation	Hydrochemistry	Geogenic contaminants
Aquifer Type 1	Recent alluvial deposits of white water rivers	$Ca\text{-}Mg\text{-}HCO_3$ Reducing pH slightly acidic - neutral	As Mn
Aquifer Type 2	Ucayali Fm.	$Na\text{-}Ca\text{-}HCO_3$ $Na\text{-}Cl\text{-}HCO_3$ Reducing pH neutral to slightly alkaline	Sporadic Mn, As
Aquifer Type 3	Iquitos Fm.	Na-Cl Oxidizing pH acidic	Al
Aquifer Type 4	Nauta Fm. Ipururo/Pebas Fm.	Na-Ca-HCO3 Oxidizing-reducing pH acidic to neutral	Sporadic Al Sporadic As, Mn

5.1. Groundwater arsenic and manganese enrichment

5.1.1. Aquifer Type 1

The hydrochemistry of Aquifer Type 1 points to reductive dissolution of Fe-(hydr)oxides as the main process leading to groundwater arsenic enrichment. The pH, the redox potential (Figure 8a), and the elevated concentrations of As, HCO_3^-, Fe, PO_4, NH_4^+, and DOC are typical for As-rich groundwater, such as that found, for example, in South and South-East Asia (Berg et al., 2008; McArthur et al., 2008; Smedley & Kinniburgh, 2002; Winkel et al., 2011), where this association has been related to As-release by microbially driven reductive dissolution of iron-(hydr)oxides (Fendorf et al, 2010; Islam et al., 2004; Mc Arthur et al., 2004).

The sandy layers of Aquifer Type 1 correspond to the uppermost alluvial floodplain aquifers of the Ucayali, Marañon, and Amazon Rivers. A high load of sediments of Andean origin has been deposited by these whitewater rivers throughout the late Quaternary, with elevated subsidence rates resulting

385 in the rapid burial of sediments. The young alluvial sediments and the infiltrating river water are rich
386 in NOM (Ertel et al., 1986) that fuels the reductive conditions in the subsurface. The poor drainage
387 enhances anoxic conditions in the aquifers. Indications of Fe-reducing subsurface conditions can
388 actually be observed after heavy rainfalls, when orange-colored groundwater ex-filtrates at the
389 riverbanks, indicating oxidation of iron-rich water. The riverbanks are used for agriculture, so
390 investigations are needed to determine if the ex-filtrating groundwater is also enriched in As, and to
391 what extent uptake by the rice plants and other crops occurs (Ravenscroft et al., 2009; Williams et
392 al., 2005).

393 Groundwater from Aquifer Type 1 had Mn ≥400 µg/L (Figure 8b), and some samples with Eh values
394 reaching 200 mV were only enriched in Mn but not in As (see Fig. 8a and 8b). This concurs with
395 reductive dissolution of Mn-oxides starting before reduction of Fe-oxides (McArthur et al., 2012;
396 Winkel et al., 2011).

397 Samples of two wells with low As-concentrations (< 5 µg/L) contained 10–20 mg/L sulfate and are
398 within a distance of less than 200m from a high-As well. Neighboring As-contaminated and As-non
399 contaminated wells are typical for As-affected basins in S-SE-Asia (e.g., Berg et al.,2008; Buschmann
400 et al., 2007; McArthur et al., 2004). This irregular pattern has been explained by local heterogeneity
401 in the subsurface (Hoque et al., 2012; McArthur et al., 2008). In our study, the wells tapping Fe-
402 reducing aquifers all showed a clearly visible orange-brown stain on the well platform caused by the
403 precipitation of Fe-(hydr)oxides. This characteristic feature has been reported in Bangladesh (Biswas
404 et al., 2012; McArthur et al., 2011,2012) and is presently seen as a widespread indicator of As
405 contaminated wells.

406 Hence, our study demonstrates that arsenic and manganese are mobilized in the unconfined aquifers
407 in the recent sediments of the floodplains of the white water rivers in Western Amazonia in Peru.

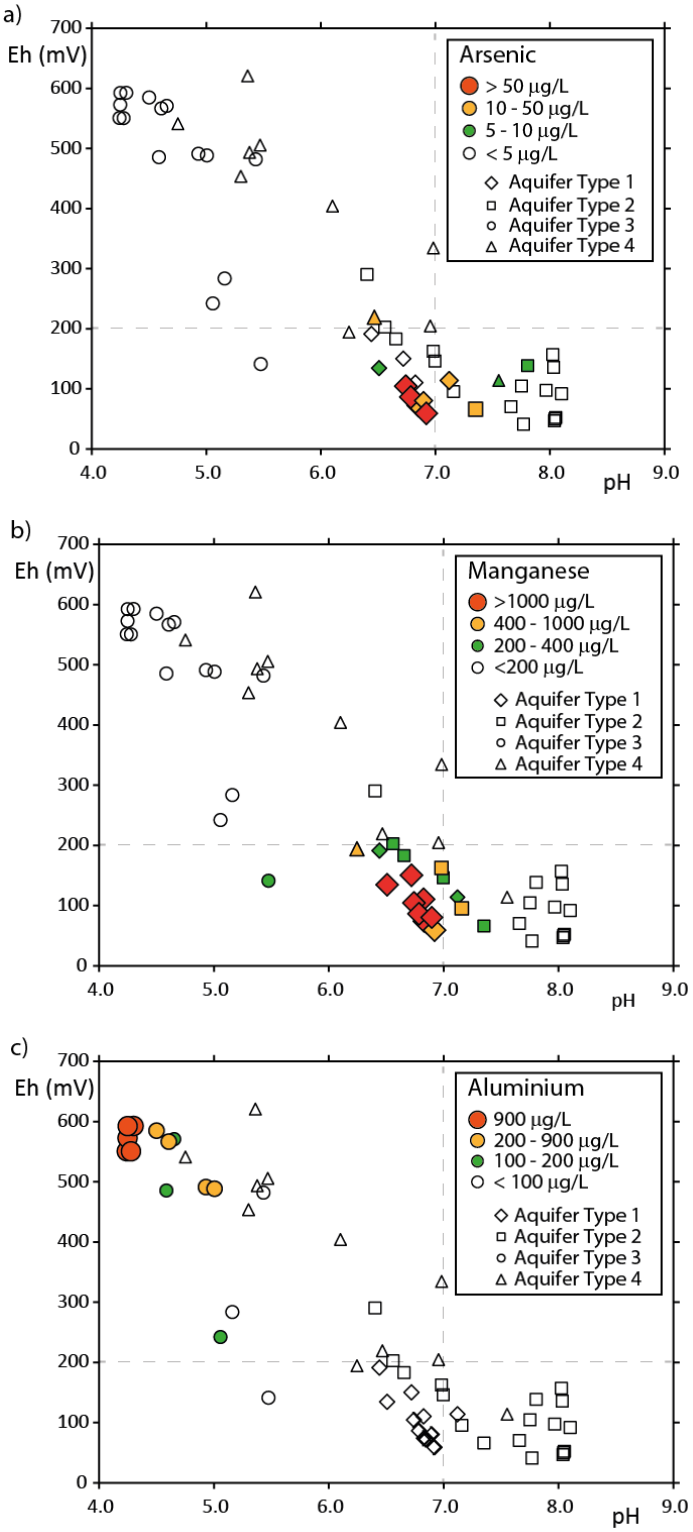

Fig. 8. Eh-pH diagram. Symbols correspond to the aquifer type, color and size of the symbols indicate concentration ranges. (a, b) High As and Mn concentrations were found in reducing groundwater of pH between 6 and 7.2, mainly in Aquifer Type 1, but also in Aquifer Types 2 and 4. (c) High concentrations of Al were detected in acidic groundwater at pH below 5 in Aquifer Type 3.

5.1.2. Aquifer Type 2

Most wells located in the region of Pucallpa on the floodplain of the Ucayali River produce groundwater with As and Mn concentrations below 10 µg/L and 400 µg/L, respectively, even though they are situated within Holocene alluvial deposits (Figure 9b). This is because most of these wells are deep and tap groundwater from Aquifer Type 2, as can be seen in the cross-section of Figure 3c. We interpret Aquifer Type 2 to consist of sandy layers of the Ucayali Fm. (see Section 4.1). The redox potential and the presence of NH_4^+ indicate reducing aquifer conditions. The pH was generally higher for groundwater from Aquifer Type 2 than from Aquifer Type 1 (Figure 5). The cations in groundwater of this aquifer type indicate evolved waters (Figure 4), thereby pointing to an increased maturity of the aquifers, with increasing Na/K and Na+K/(Ca+Mg+Na+K) ratios correlating with increasing pH. The wells located east of the Ucayali River produce saline, Na-Cl waters. Here, possible explanations for the observed shift towards Na-Cl waters (Figure 4) are an inflow of salty water from older formations, where gypsum and salt have been described (De La Cruz et al., 1997a,b; Guzmán & Núñez, 1998a) or dissolution of hitherto undescribed evaporate minerals in the Ucayali Fm.

Within Aquifer Type 2, we observe a pronounced change in Mn and Fe-concentrations (Figures 7a and 7b) at pH ~7.5 (see Figure 8b). Groundwater with pH values above this value had Mn <200 µg/L and Fe-concentrations <0.1 mg/L, whereas groundwater of pH <7.5 had Mn- and Fe-concentrations up to 500 µg Mn/L and 1.1 mg Fe/L, indicating Mn and Fe-reduction, but resulting in lower dissolved Fe and Mn concentrations than in groundwater from Aquifer Type 1. Groundwater from Aquifer Type 2 had clearly lower concentrations of N and DOC when compared to groundwater of Aquifer Type 1 (Figure 6). The several-meters-thick clay layers that are described in the Ucayali Fm. might hinder the inflow of NOM (electron donor) that is crucial for triggering reductive dissolution of Fe and Mn(hydr)oxides (Lovley & Chapelle, 1995; McArthur et al., 2004; Petrunic et al., 2005). Some wells emitted a rotten egg smell of hydrogen sulfide from freshly pumped groundwater, which is an indication for sulfate reduction taking place in at least part of Aquifer Type 2. Interestingly, samples of Aquifer Type 2 contained significantly higher Mo concentrations when compared to the other

441 aquifer types (Figure 6), with the highest concentrations (Mo >6 µg/L) corresponding to the samples
442 with pH >7.5, and hence with the lower Fe concentrations. This differs from observations made
443 previously, for example in West Bengal, where elevated concentrations of Mo have been related to
444 elevated concentrations of As and Fe (Hoque et al.,2012).

445 Fe(III) reduction and sulfate reduction depend on pH and the stability of the Fe phases (Postma &
446 Jacobsen, 1996), and both might occur concurrently in the same aquifer. Determining which
447 processes are dominant in this aquifer type lies beyond the scope of this paper.

448 **5.1.3. Aquifer Type 4**

449 All aquifers of the older formations are grouped in Aquifer Type 4. These sedimentary formations are
450 heterogeneous (see section 4.1), which is also reflected in the hydrochemistry. In our study, the As
451 and Mn concentrations did not exceed 10 µg As/L and 450 µg Mn/L. Slightly higher concentrations of
452 up to 26 µg As/L and 560 µg Mn/L were reported by Rebata-H et al. (2009). Mobilization of As and
453 Mn in groundwater is limited to parts of the Pebas and Ipururo Formations. Reducing conditions at
454 near neutral pH prevail in the aquifers that are embedded in the blue-colored clay layers of the Pebas
455 or Ipururo Fm., where lignite and carbonate-rich layers are present (see sections 2.1 and 2.2). These
456 aquifer conditions can lead to mobilization of redox-sensitive elements, such as Fe, Mn, and As, by
457 similar processes as occur in the young alluvial aquifers (i.e., Aquifer Type 1). Oxidation of Fe-sulfides,
458 related to seasonally moving groundwater tables, might also lead to mobilization of As and Fe in
459 sediments containing reduced Fe minerals (Ravenscroft et al., 2009), such as pyrite in the Pebas Fm.

460 **5.2. Groundwater aluminum enrichment (Aquifer Type 3)**

461 High concentrations of Al were only observed in groundwater of Aquifer Type 3, which is an
462 unconfined aquifer in the Iquitos Fm. that consists of almost pure quartz sands (Räsänen et al., 1998;
463 Sánchez et al., 1999a). No buffering of the pH can occur when acidic water infiltrates a pure sand
464 aquifer in which carbonaceous minerals are scarce, such that the groundwater remains acidic
465 (Edmunds et al., 1992). The solubility of Al increases with increasing acidity (Hansen & Postma, 1995).

Dissolution of Al-rich minerals, such as gibbsite and kaolinite, results in an increase of Al in groundwater and in pH buffering (Nordstrom & Ball, 1986). In our samples, buffering resulted in a minimum pH of 4.2 (see Figures 7e and 8c). Groundwater aluminum enrichment in podzols or pure sand aquifers is well known and has been described in the Amazon region (e.g., Lucas et al., 2012) and elsewhere in the world (e.g., Edmunds et al., 1992, Kjöller et al., 2004). Acid rain and/or infiltration of surface water enriched in humic acids are generally the sources of initial acidity (Edmunds et al., 1992).

The presence of acidic, Al-rich groundwater is hence not only related to the Iquitos Fm., but also to pure sand sediments or podzolic soils in which blackwater rivers, such as the Nanay River, originate. Unconfined aquifers in the Nauta Fm. (Aquifer Type 4) might also be vulnerable to Al enrichment. Al-rich minerals, such as kaolinite and Al-chlorite, have been described in sands of the Nauta Fm., indicating that parts of the Nauta Fm. are highly weathered (Kauffman et al., 1998; Martínez et al., 1999). In our survey, groundwater from Aquifer Type 4 had a minimum pH of 4.8 and Al-concentrations of max. 60 µg/L, although Rebata-H et al. (2009) observed concentrations of up to 600 µg/L at a pH of 4.2.

Groundwater from wells tapping the Iquitos Fm., but located in the actual flooding zone of the Amazon River, have different characteristics. Here, an annually deposited fresh layer of silt from the Amazon River acts as a buffer to infiltrating water, resulting in more reducing groundwater with a higher pH and subsequent mobilization of Fe and Mn. The possible co-mobilization of As requires further investigation.

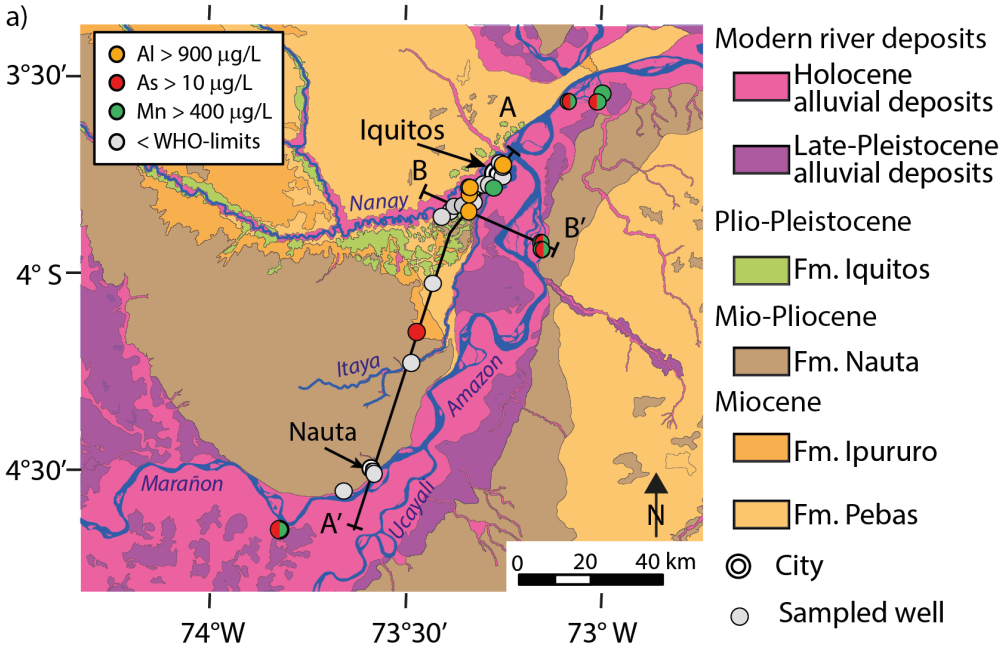

486

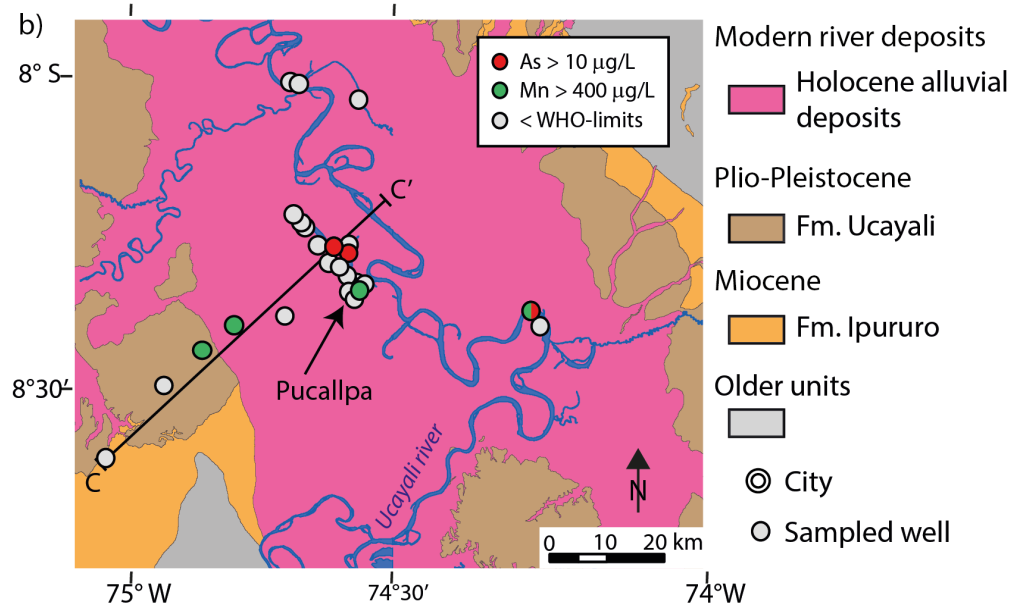

487

488 **Fig. 9.** Maps highlighting Al, As, and Mn concentrations above the WHO guideline values in a) the
489 region of Iquitos, and b) the region of Pucallpa. The groundwaters exceeding the WHO health-based
490 value (WHO, 2011) of 900 µg/L for Al are all from Aquifer Type 3 of the Iquitos Fm. (Figure a). Wells
491 with samples exceeding the WHO-guideline values (WHO, 2011) of 10 µg/L for As or 400 µg/L for Mn
492 are mainly located on the recent alluvial deposits of the white water rivers (Modern river deposits).
493 References are according to Figure 2.

5.3. Implications for the use of groundwater as drinking water resource in Western Amazonia

In more than one third of the studied groundwater samples, the concentrations of Al, As, and/or Mn exceeded the WHO-guideline or health based values (WHO, 2011). Chronic arsenic exposure can lead to skin lesions, hyperkeratosis, melanosis, skin cancer, and internal organ cancer (Hughes, 2002; Kapaj et al., 2006; Smith et al., 2000; Yoshida et al., 2004). Case studies have indicated that chronic exposure to elevated concentrations of Mn may lead to neurotoxicity, especially in young children (Bouchard et al., 2011; Wasserman et al., 2006). Ljung and Vahter (2007) argued that the health-based guideline of 400 µg/L set by the WHO is outdated and should be revised to a lower value. Chronic uptake of Al through drinking water has been linked with Alzheimer's disease and other neurological disorders, although this is still a matter of debate (for an overview, see Bondy, 2016; Walton, 2014).

Hence, the presence of geogenic contaminants points to an urgent need to assess the groundwater quality throughout Western Amazonia. Mitigation measures are required, including raising the awareness of well owners and the authorities and NGOs in charge of well construction. Groundwater quality testing should include the analysis of the trace elements Al, As, and Mn. Contaminated groundwater clearly needs treatment before consumption, however solutions can be adapted to local conditions. We recommend an investigation of the potential negative health effects of chronic intake of the contaminated water, taking into account local dietary habits, which can help mitigate or exacerbate health impacts.

Our study highlights the vulnerability of two types of aquifers to geogenic groundwater contamination in Western Amazonia (Table 2). The first type includes the aquifers in the Modern river deposits of the floodplains of the whitewater rivers (Aquifer Type 1), where As and Mn are mobilized by reductive dissolution. The second type comprises the unconfined pure sand aquifers (Aquifer Type 3), where aluminum is enriched due to acidic groundwater conditions. These conditions are not only limited to the white sands of the Iquitos Fm., but also occur in similar highly

519 weathered or pure sand formations throughout the Amazon Basin and especially in the catchments
520 of blackwater rivers.

521 The deeper or older aquifers (Aquifer Types 2 and 4, Table 2) were rarely affected by geogenic
522 groundwater contamination. The wells tapping the aquifers of the Ucayali Fm. mainly produce
523 groundwater of good quality, however the detection of As >10 µg/L and Mn concentrations >200
524 µg/L highlights that wells in this formation should be monitored. Our study also showed that
525 groundwater from aquifers of the Miocene Pebas and Ipururo formations may occasionally have
526 elevated concentrations of Mn and As. Linking water quality with specific parts of the sedimentary
527 formations grouped in Aquifer Type 4 will need further research. The wells of larger settlements and
528 cities tap groundwater from Aquifer Type 4, which therefore represents important drinking water
529 resources in Western Amazonia. Hence, to avoid aquifers with geogenic contaminants, an important
530 future step will be the determination of the minimal and maximal depths corresponding to non-
531 contaminated aquifers.

532 **6. Conclusion**

533 Our study raises an initial awareness of the presence of geogenic contaminants in the groundwater
534 resources of Western Amazonia. We show that the hydrogeochemical characteristics of groundwater
535 in the Peruvian Western Amazonia are related to the river type and the sedimentary unit. The data
536 demonstrate arsenic and manganese contamination under reducing conditions in unconfined
537 aquifers of the young floodplains of the whitewater rivers, whereas acidic groundwater in sandy
538 deposits in the catchments of blackwater rivers contain high concentrations of aluminum. The
539 health-threatening concentrations of arsenic, manganese, and aluminum detected in almost half of
540 the groundwater samples call for a thorough investigation of groundwater quality throughout the
541 whole region.

ACKNOWLEDGMENTS

We are very thankful to the DESA in Loreto and in Ucayali and the ETRAS-section of PAHO in Lima for assistance during field work, and to all well-owners for giving us permission to sample. We are grateful to the AuA laboratory and Numa Pfenninger at Eawag for elemental analysis, to Lenny Winkel, Joel Podgorski and Anja Bretzler for manuscript feedback, and to Fredy Jaimes from INGEMMET (Lima, Peru) for discussion about regional geology and access to unpublished documentation. The authors would like to thank the reviewers for their constructive comments on the manuscript. This project benefited from financial support through a 2015 Seed Money Grant for Latin America - Swiss Bilateral Program, from CODEV-EPFL and a Swiss National Science Foundation (SNSF) Grant (n° 165913).

REFERENCES

Amini M., Abbaspour K. C., Berg M., Winkel L., Hug S.J., Hoehn E., Yang H., Johnson A. (2008). Statistical modeling of global geogenic arsenic contamination in groundwater. Environmental Science & Technology, 42 (10), 3669-3675.

Berg M., Tran H.C., Nguyen T.C., Pham H.V., Schertenleib R., Giger W., (2001). Arsenic contamination of groundwater and drinking water in Vietnam: a human health threat. Environ. Sci. Technol. 35 (13), 2621–2626.

Berg M., Trang P.T.K., Stengel C., Buschmann J., Viet P.H., Van Dan N., Giger W. and Stüben D. (2008). Hydrological and sedimentary controls leading to arsenic contamination of groundwater in the Hanoi area, Vietnam: The impact of iron-arsenic ratios, peat, river bank deposits, and excessive groundwater abstraction. Chemical Geology 249 (1-2), 91–112.

564 Biswas A., Nath B., Bhattacharya P., Halder D., Kundu A.K., Mandal U., Mukherjee A., Chatterjee D.
565 and Jacks G. (2012). Testing Tubewell Platform Color as a Rapid Screening Tool for Arsenic and
566 Manganese in Drinking Water Wells. Environ. Sci. Technol. 46 (1), 434–440.

567 Bondy S.C. (2016). Low levels of aluminum can lead to behavioral and morphological changes
568 associated with Alzheimer's disease and age-related neurodegeneration. NeuroToxicology 52, 222-
569 229.

570 Bouchard M.F., Sauve S., Barbeau B., Legrand M., Brodeur M.E., Bouffard T., Limoges E., Bellinger
571 D.C. and Mergler, D. (2011). Intellectual Impairment in School-Age Children Exposed to Manganese
572 from Drinking Water. Environmental Health Perspectives 119 (1), 138-143.

573 Bundschuh J., Litter M. I., Parvez F., Roman-Ross G., Nicolli, H. B., Jean, J. S., Liu, C. W., Lopez, D.,
574 Armienta, M. A., Guilherme, L. R. G., Cuevas, A. G., Cornejo, L., Cumbal, L., Toujaguez, R. (2012). One
575 century of arsenic exposure in Latin America: A review of history and occurrence from 14 countries.
576 Science of the Total Environment 429, 2-35.

577 Buschmann J., Berg M., Stengel C. and Sampson M. (2007). Arsenic and manganese contamination of
578 drinking water resources in Cambodia: Coincidence of risk areas with low relief topography. Environ.
579 Sci. Technol. 41 (7), 2146-2152.

580 Buschmann J., Berg M., Stengel C., Winkel L., Sampson M.L., Trang P.T.K., Viet P.H. (2008).
581 Contamination of Drinking Water Resources in the Mekong Delta Floodplains: Arsenic and Other
582 Trace Metals Pose Serious Health Risks to Population. Environment International 34, 756–764.

583 Campbell K.E., Frailey C.D. and Romero-Pittman L. (2006).The Pan-Amazonian Ucayali Peneplain, late
584 Neogene sedimentation in Amazonia, and the birth of the modern Amazon River system.
585 Palaeogeography, Palaeoclimatology, Palaeoecology 239 (1-2), 166–219.

586 De La Cruz B. N. (1997a). Mapa Geológico del cuadrángulo de Pucallpa. Edición-1 Hoja (1954) 17-n.
587 Carta geológica del Perú 1:100.000. INGEMMET, Peru.

De la Cruz B.N. (1997b). Mapa Geológico del cuadrángulo de Nuevo Utiquinía. Edición-1 Hoja (2054) 17-ñ. Carta geológica del Perú 1:100.000. INGEMMET, Peru.

De La Cruz W.J. and Raymundo S.T. (1997). Mapa Geológico del cuadrángulo de Santa Rosa. Edición-1 Hoja (1953) 18-n. Carta geológica del Perú 1:100.000. INGEMMET, Peru.

De La Cruz J., Lara M. and Raymundo T. (1997a). Geología de los cuadrángulos 18-m, 18-n, 19-m, 19-n. INGEMMET, Boletín, Serie A, 98, pp.118.

De La Cruz N., Zedano J. and Zapata A. (1997b). Geología de los cuadrángulos 16-n, 16-ñ, 16-o, 17-n, 17-ñ, 17-o, 17-p. INGEMMET, Boletín, Serie A, 102, pp.156.

Dumont J.F., Lamotte S. and Fournier M. (1988). Neotectónica del Arco de Iquitos (Jenaro Herrera, Perú). Boletín de la Sociedad Geológica del Perú 77,7-17.

Edmunds W. M., Kinniburgh D. G. and Moss P. D. (1992). Trace-metals in interstitial waters from sandstones – acidic inputs to shallow groundwaters. Environmental Pollution 77 (2-3), 129-141.

Ertel J. R., Hedges J. I., Devol A. H., Richey J. E. and Ribeiro M. D. G. (1986). Dissolved humic substances of the Amazon River system. Limnology and Oceanography 31 (4), 739-754.

Fendorf S., Michael H.A. and van Geen A. (2010). Spatial and temporal variations of groundwater arsenic in South and Southeast Asia. Science 328 (5982), 1123-1127.

Flores-P.S., Gómez-R.E. and Kalliola R. (1998). Características generales de la zona de Iquitos. In: Kalliola R. & Flores-P. S. (eds.) Geoecología y desarrollo Amazónico: Estudio integrado en la zona de Iquitos, Perú; Annales Universitatis Turkuensis Ser. A II, 114.

Guzmán A. and Núñez S. (1998a). Geología de los cuadrángulos 18-ñ, 18-o, 19-ñ, 19-o, 20-ñ, 20-o. INGEMMET, Boletín Serie A, 114, pp.133.

Guzmán M.A. and Núñez J.S. (1998b). Mapa Geológico del cuadrángulo de Masisea. Edición-1 Hojas (2053) 18-ñ. Carta geológica del Perú 1:100.000. INGEMMET, Peru.

611 Hansen B.K. and Postma D. (1995). Acidification, buffering, and salt effects in the unsaturated zone of
612 a sandy aquifer, Klosterhede, Denmark. Water Resources Research 31 (11), 2795-2809.

613 Hoorn C., Wesselingh F.P., ter Steege H., Bermudez M.A., Mora A., Sevink J., Sanmartin I., Sanchez-
614 Meseguer A., Anderson C.L., Figueiredo J.P., Jaramillo C., Riff D., Negri F.R., Hooghiemstra H.,
615 Lundberg J., Stadler T., Särkinen T and Antonelli A., (2010). Amazonia Through Time: Andean Uplift,
616 Climate Change, Landscape Evolution, and Biodiversity. Science 330 (6006), 927-931.

617 Hoque M. A., McArthur J. M. and Sikdar P. K. (2012). The palaeosol model of arsenic pollution of
618 groundwater tested along a 32 km traverse across West Bengal, India. Science of the Total
619 Environment 431, 157-165.

620 Hughes M.F. (2002). Arsenic toxicity and potential mechanisms of action. Toxicology letters 133, 1-6.

621 INEI (2012): Perú: Estimaciones y Proyecciones de Población Total por Sexo de las Principales
622 Ciudades, 2000-2015. Boletín Especial N°23. Instituto Nacional de Estadística e informática, Lima, pp.
623 50.

624 INGEMMET (1999). Mapa Geológico del Perú Escala 1:1 000 000. Digitalized version from 2010,
625 GEOCATMIN: PERU GEOLOGIA NACIONAL 1:1M. Instituto Geológico Minero y Metalurgico. Direccion
626 de Geología Regional. Lima, Peru.

627 INRENA (1998). Inventario y evaluación de las fuentes de las aguas subterránea de la ciudad de
628 Pucallpa y Yarinacocha. Informe final. Ministerio de Agricultura, Pucallpa, Perú.

629 INRENA (2006). Inventario de fuentes de agua subterránea Iquitos. Informe final. Ministerio de
630 Agricultura, Lima, Perú.

631 Islam F. S., Gault A. G., Boothman C., Polya D. A., Charnock J. M., Chatterjee D. and Lloyd J. R. (2004).
632 Role of metal-reducing bacteria in arsenic release from Bengal delta sediments. Nature 430 (6995),
633 68-71.

634 Junk W. J., Piedade M. T. F., Schongart J., Cohn-Haft M., Adeney J. M. and Wittmann F. (2011). A
635 classification of major naturally-occurring Amazonian Lowland wetlands. Wetlands 31 (4), 623-640.

636 Kalliola R., Linna A., Puhakka M., Salo J. And Räsänen, M. (1993). Mineral nutrients in fluvial
637 sediments from the Peruvian Amazon. Catena 20 (3), 333-349.

638 Kapaj S., Peterson, H., Liber K. and Bhattacharya P. (2006). Human health effects from chronic arsenic
639 poisoning - a review. Journal of Environmental Science and Health, Part A, 41, 2399-2428.

640 Kauffman S., Paredes-A. G. and Marquina R. (1998). Suelos de la zona de Iquitos. In: Kalliola R. &
641 Flores-P. S. (eds.) Geoecología y desarrollo Amazónico: Estudio integrado en la zona de Iquitos, Perú;
642 Annales Universitatis Turkuensis Ser. A II, 114,139-229.

643 Kjöller C., Postma D. and Larsen F. (2004). Groundwater Acidification and the Mobilization of Trace
644 Metals in a Sandy Aquifer. Environ. Sci. Technol. 38, 2829-2835.

645 Klinge H. (1967). Podzol soils: A source of blackwater rivers in Amazonia. Atas Simp. Biota Amaz.
646 Belem 3, 117-125.

647 Ljung K. and Vahter M. (2007). Time to re-evaluate the guideline value for manganese in drinking
648 water? Environmental Health Perspectives 115 (11), 1533-1538.

649 Lovley D.R. and Chapelle F.H. (1995). Deep subsurface microbial processes. Reviews of Geophysics 33
650 (3), 365-381.

651 Lucas Y., Montes C.R., Mounier S., Cazalet M.L., Ishida D., Achard R., Garnier C., Coulomb B. and Melfi
652 A.J. (2012). Biogeochemistry of an Amazonian podzol-ferralsol soil system with white kaolin.
653 Biogeosciences 9 (9), 3705-3720.

654 Marengo J.A. (1998). Climatología de la Zona de Iquitos, Peru. In: Kalliola R. & Flores-P. S. (eds.)
655 Geoecología y desarrollo Amazónico: Estudio integrado en la zona de Iquitos, Perú; Annales
656 Universitatis Turkuensis Ser. A II, 114,35-57.

657 Martínez W., Morales M., Díaz G., Milla D., Montoya C., Huayhua J., Romero L. and Raymundo T.
658 (1999). Geología de los cuadrángulos 5-n, 5-ñ, 5-o, 6-n, 6-ñ, 6-o, 7-n, 7-ñ, 7-o, 8-n, 8-ñ, 8-o, 9-n, 9-ñ,
659 9-o, 10-n, 10-ñ y 10-o. INGEMMET, Boletín Serie A, 131, pp.354.

660 Martinez V.W. and Morales R.M. (1999a). Mapa Geológico del cuadrángulo de Libertad. Edición-1
661 Hoja (2063) 8-ñ. Carta geológica del Perú 1:100.000. INGEMMET, Peru.

662 Martinez V.W. and Morales R.M. (1999b). Mapa Geológico del cuadrángulo de Rio Nanay. Edición-1
663 Hoja (2163) 8-o. Carta geológica del Perú 1:100.000. INGEMMET, Peru.

664 McArthur J. M., Banerjee D.M., Hudson-Edwards K.A., Mishra R., Purohit R., Ravenscroft P., Cronin A.,
665 Howarth R.J., Chatterjee A., Talukder T., Lowry D., Houghton S. and Chadha D.K. (2004). Natural
666 organic matter in sedimentary basins and its relation to arsenic in anoxic groundwater: The example
667 of West Bengal and its worldwide implications. Appl. Geochem. 19, 1255– 1293.

668 McArthur J. M., Ravenscroft P., Banerjee D.M., Milsom J., Hudson-Edwards K.A., Sengupta S., Bristow
669 C., Sarkar A., Tonkin S. and Purohit R. (2008). How paleosols influence groundwater flow and arsenic
670 pollution: A model from the Bengal Basin and its worldwide implication. Water Resources Research,
671 44 (11), W11411.

672 McArthur J. M., Nath B., Banerjee D. M., Purohit R. and Grassineau N. (2011). Palaeosol Control on
673 Groundwater Flow and Pollutant Distribution: The Example of Arsenic. Environmental Science &
674 Technology 45 (4), 1376-1383.

675 McArthur J. M., Sikdar P. K., Nath B., Grassineau N., Marshall J. D. and Banerjee D. M. (2012).
676 Sedimentological Control on Mn, and Other Trace Elements, In Groundwater of the Bengal Delta.
677 Environmental Science & Technology 46 (2), 669-676.

678 Meharg A. A., Scrimgeour C., Hossain S.A., Fuller K., Cruickshank K., Williams P.N. and Kinniburgh D.G.
679 (2006). Codeposition of organic carbon and arsenic in Bengal Delta aquifers. Environ. Sci. Technol. 40
680 (16), 4928–4935.

681 Meng X. and Wang W. (2008). Speciation of Arsenic by disposable cartridges. Proceedings of the
682 Third International Conference on Arsenic Exposure and Health Effects, Soc. Environ. Geochem. and
683 Health, Univ Colorado at Denver.

684 Monge R. and Valencia M. (1999a). Mapa Geológico del cuadrángulo de Tamshiyacu. Edición-1 Hoja
685 (2262) 9-p. Carta geológica del Peru 1:100.000. INGEMMET, Peru.

686 Monge R. and Valencia M. (1999b). Mapa Geológico del cuadrángulo de Rio Tamshiyacu. Edición-1
687 Hoja (2362) 9-q. Carta geológica del Peru 1:100.000. INGEMMET, Peru.

688 Monge R. and Valencia M. (1999c). Mapa Geológico del cuadrángulo de Rámon Castilla. Edición-1
689 Hoja (2261) 10-p. Carta geológica del Peru 1:100.000. INGEMMET, Peru.

690 Monge R. and Valencia M. (1999d). Mapa Geológico del cuadrángulo de Rio Yavari Mirin. Edición-1
691 Hoja (2361) 10-q. Carta geológica del Peru 1:100.000. INGEMMET, Peru.

692 Mora A., Baby P., Roddaz M., Parra M., Christophoul F, Brusset S., Hermoza W. and Espurt N. (2010).
693 Tectonic history of the Andes and sub-Andean zones: implications for the development of the
694 Amazon drainage basin. In: Hoorn C. and Wesselingh F.P. (Eds.). Amazonia: Landscape & Species
695 Evolution: A Look into the Past. Blackwell Publishing Ltd. West Sussex, pp. 38-60.

696 Nickson R., McArthur J.M., Burgess W., Ahmed K.M., Ravenscroft P. and Rahman M. (1998). Arsenic
697 poisoning of Bangladesh groundwater. Nature 395, 338.

698 Nordstrom D.K. and Ball J.W. (1986). The geochemical behavior of aluminum in acidified surface
699 waters. Science 232 (4746), 54-56.

700 Paredes-G. A., Kauffman S. and Kalliola, R. (1998). Suelos aluviales recientes de la zona de Iquitos-
701 Nauta. In: Kalliola R. & Flores-P. S. (eds.) Geoecología y desarrollo Amazónico: Estudio integrado en la
702 zona de Iquitos, Perú; Annales Universitatis Turkuensis Ser. A II, 114,231-251.

703 Petrunic B. M., MacQuarrie K. T. B. and Al T. A. (2005). Reductive dissolution of Mn oxides in river-
704 recharcred aquifers: a laboratory column study. Journal of Hydrology 301 (1-4), 163-181.

705 Postma D. and Jacobsen R. (1996). Redox zonation: Equilibrium constraints on the Fe(III)/SO4-
706 reduction interface. Geochimica et Cosmochimica Acta 60 (17), 3169-3175.

707 Postma D., Larsen F., Thai N.T., Trang P.T.K., Jakobsen R., Nhan P.Q., Long T.V., Viet P.H. and Murray
708 A.S. (2012). Groundwater arsenic concentrations in Vietnam controlled by sediment age. Nature
709 Geosciences 5 (9), 656–661.

710 Puhakka M., Kalliola R., Rajasilta M. and Salo J. (1992). River Types, Site Evolution and Successional
711 Vegetation Patterns in Peruvian Amazonia. Journal of Biogeography 19 (6), 651-665.

712 Räsänen M., Neller R., Salo J. and Jugnger H. (1992). Recent and ancient fluvial deposition systems in
713 the Amazonian foreland basin, Peru. Geol. Mag. 129 (3), 293-306.

714 Räsänen, M., Linna, A., Irion, G., Rebata, L., Wesselingh, F. & Vargas, R. (1998). Geología y geoformas
715 de la zona de Iquitos. In: Kalliola R. & Flores-P. S. (eds.) Geoecología y desarrollo Amazónico: Estudio
716 integrado en la zona de Iquitos, Perú; Annales Universitatis Turkuensis Ser. A II, 114, 59-137.

717 Ravenscroft P., McArthur J. M. and Hoque B. A. (2001). Geochemical and palaeohydrological controls
718 on pollution of groundwater by arsenic. In: Arsenic Exposure and Health Effects IV; Chappell W. R.,
719 Abernathy, C. O. & Calderon, R. L. (eds.), Elsevier Science Bv, Amsterdam, 53-77.

720 Ravenscroft P., Brammer H. and Richards K.S. (2009). Arsenic Pollution: A Global Synthesis. Wiley-
721 Blackwell, West Sussex, 579 p.

722 Rebata-H L.A., Räsänen M.E., Gingras M.K., Vieira V., Barberi M. and Irion G. (2006). Sedimentology
723 and ichnology of tide-influenced Late Miocene successions in western Amazonia: The gradational
724 transition between the Pebas and Nauta formations. Journal of South American Earth Sciences 21 (1-
725 2), 96–119.

726 Rebata-H. L.A., Korkka-Niemi K., Heikkinen P-M. and Räsänen M.E. (2009). Hydrogeochemical
727 characterisation of the Miocene Pebas and Nauta formations in Peruvian Amazonia. Boletín de la
728 Sociedad Geológica del Perú 103, 125-151.

729 Roddaz M., Hermoza W., Mora A., Baby P., Parra M., Christophoul F., Brusset S. and Espurt N. (2010).
730 Cenozoic sedimentary evolution of the Amazonian foreland basin system. In: Hoorn C. and
731 Wesselingh (Eds.) Amazonia: Landscape & Species Evolution: A Look into the Past. Blackwell
732 Publishing Ltd. West Sussex, pp. 61-88.

733 Romero P.L. and Raymundo S.T. (1999a). Mapa Geológico del cuadrángulo de Yacumama. Edición-1
734 Hoja (2062) 9-ñ. Carta geológica del Perú 1:100.000. INGEMMET, Peru.

735 Romero P.L. and Raymundo S.T. (1999b). Mapa Geológico del cuadrángulo de Rio Itaya. Edición-1
736 Hoja (2162) 9-o. Carta geológica del Peru 1:100.000. INGEMMET, Peru.

737 Romero P.L. and Raymundo S.T. (1999c). Mapa Geológico del cuadrángulo de Chapajilla. Edición-1
738 Hoja (2061) 10-ñ. Carta geológica del Peru 1:100.000. INGEMMET, Peru.

739 Romero P.L. and Raymundo S.T. (1999d). Mapa Geológico del cuadrángulo de Nauta. Edición-1 Hoja
740 (2161) 10-o. Carta geológica del Peru 1:100.000. INGEMMET, Peru.

741 Rossetti D.F. (2014). The role of tectonics in the late Quaternary evolution of Brazil's Amazonian
742 landscape. Earth-Science Reviews 139, 362-389.

743 Rüegg W. and Rosenzweig A. (1949). Contribución a la geología de las formaciones modernas de
744 Iquitos y de la Amazonia Superior. Boletín de la Sociedad Geológica del Perú 25 (2), 1-26.

745 Sánchez A., Chira J., Romero D., De la Cruz J., Herrera I., Cervante J., Monge R., Valencia M. and
746 Cuba, A. (1999a). Geología de los cuadrángulos 4-p,5-p, 5-q, 5-r, 6-p, 6-q, 6-r, 7-p, 7-q, 7-r, 8-p, 8-q, 8-
747 r,9-p, 9-q, 9-r, 10-p, 10-q y 10-r. INGEMMET, Boletín, Serie A, 132, pp.290.

748 Sánchez F.A., Chira F.J. and Romero F.D. (1999b). Mapa Geológico del cuadrángulo de Iquitos.
749 Edición-1 Hoja (2263) 8-p. Carta geológica del Perú 1:100.000. INGEMMET, Peru.

750 Sánchez F.A., Chira F.J. and Romero F.D. (1999c). Mapa Geológico del cuadrángulo de Rio Maniti.
751 Edición-1 Hoja (2363) 8-q. Carta geológica del Perú 1:100.000. INGEMMET, Peru.

752 Sioli H. (1956). Über Natur und Mensch im brasilianischen Amazonasgebiet. Erdkunde 10 (2), 89–109.

753 Smedley P.L. and Kinniburgh D.G. (2002). A review of the source, behavior and distribution of arsenic
754 in natural waters. Applied Geochemistry 17, 517–568.

755 Smith A.H., Lingas E.O. and Rahman M. (2000). Contamination of drinking water by arsenic in
756 Bangladesh: A public health emergency. Bulletin World Health Organization 78, 1093-1102.

757 Stüben D., Berner Z., Chandrasekharam D. and Karmakar J. (2003). Arsenic enrichment in
758 groundwater of West Bengal, India: geochemical evidence for mobilization of As under reducing
759 conditions. Applied Geochemistry 18 (9), 1417-1434.

760 Syvitski J. P. M., Cohen S., Kettner A. J. and Brakenridge G. R. (2014). How important and different are
761 tropical rivers? - An overview. Geomorphology 227, 5-17.

762 UNEP (2004). Barthem, R. B., Charvet-Almeida, P., Montag, L. F. A. and Lanna, A.E. Amazon Basin,
763 GIWA Regional assessment 40b. University of Kalmar, Kalmar, Sweden.

764 Walton J.R. (2014). Chronic Aluminum Intake Causes Alzheimer's Disease: Applying Sir Austin
765 Bradford Hill's Causality Criteria. Journal of Alzheimer's Disease 40, 765–838.

766 Wasserman, G. A., Liu, X., Parvez, F., Ahsan, H., Levy, D., Factor-Litvak, kline J., van Geen A.,
767 Slavkovich V., Lolacono N.J., Cheng Z.Q., Zheng Y. and Graziano, J. H. (2006). Water Manganese
768 Exposure and Children's Intellectual Function in Araihazar, Bangladesh. Environmental Health
769 Perspectives, 114(1), 124-129.

770 Williams P. N., Price A. H., Raab A., Hossain S. A., Feldmann J. and Meharg A. A. (2005). Variation in
771 arsenic speciation and concentration in paddy rice related to dietary exposure. Environmental
772 Science & Technology 39 (15), 5531-5540.

773 Winkel L., Berg M., Amini M., Hug S.J. and Johnson A.C. (2008). Predicting groundwater arsenic
774 contamination in Southeast Asia from surface parameters. Nature Geoscience 1 (8), 536-542.

775 Winkel L.H.E., Trang P.T.K., Lan M.V., Stengel C., Amini M., Ha N.T., Viet P.H. and Berg M. (2011).
776 Arsenic pollution of groundwater in Vietnam exacerbated by deep aquifer exploitation for more than
777 a century. Proceedings of the National Academy of Sciences of the USA 108 (4), 1246-1251.

778 WHO (2011). Guidelines for Drinking-Water Quality, 4rd ed.; Geneva

779 Yoshida T., Yamauchi H. and Fan Sun G. (2004). Chronic health effects in people exposed to arsenic
780 via the drinking water: dose- response relationships in review. Toxicology and Applied
781 Pharmacology 198(3), 243–252.

782